Preliminary Identification of a Dynamical Plant Model for the Jason 2 Underwater Robotic Vehicle

David A. Smallwood and Louis L. Whitcomb*

Abstract

This paper reports the experimental identification of a finite-dimensional dynamical plant model for the Jason 2 Remotely Operated underwater Vehicle. The experiments were conducted in collaboration with the Woods Hole Oceanographic Institution during sea-trials in July 2002. A least-squares method is employed to identify decoupled single degree-of-freedom plant dynamical models for the X, Y, Z, and Heading degrees-of-freedom from experimental data. Performance of the identified plant dynamical model is evaluated by directly comparing simulations of the identified plant model to the experimentally observed motion data of the actual vehicle.

1 Introduction

This paper first reports an experimentally identified finite-dimensional non-linear dynamical models for the Jason 2 Remotely Operated underwater Vehicle (ROV). Jason 2 is a 6500 meter ROV developed and operated with NSF support for use by the U.S. Oceanographic Community by the National Deep Submergence Facility (NDSF) of the Woods Hole Oceanographic Institution (WHOI). Second, it reports an experimentally identified estimate for the coefficient of quadratic drag in the vertical degree of freedom. The methodology followed has previously been employed in [11] for work performed using the JHUROV [9]. These dynamical models will serve as the basis for implementing a class of non-linear model-based controllers [12] to be used on Jason 2.

This paper is organized as follows: First a brief background is provided. Second, Section 2.2 reviews the standard least-squares method used to identify the plant model parameters. Third, Section 3 reports the experimental setup. Fourth, the experimental results are presented in Section 4.

*Smallwood and Whitcomb are with the Department of Mechanical Engineering, The Johns Hopkins University, Baltimore, Maryland, 21218, USA, email: Smallwood@jhu.edu, llw@jhu.edu.

2 Background

This Section first reviews the finite-dimensional model employed in Section 2.1. Second, in Section 2.2, it reviews the least-squares technique used to experimentally identify the plant model parameters.

2.1 Finite-Dimensional Dynamical Modeling of Marine Vehicles

Most reported finite-dimensional approximate plant models for holonomic (fully actuated) underwater vehicles take the following general form

$$\begin{aligned} \vec{\tau}(t) &= M(\vec{x}_w(t), \vec{v}(t))\dot{\vec{v}}(t) + \\ &\quad d(\vec{x}_w(t), \vec{v}(t)) + b(\vec{x}_w(t)) \end{aligned} \tag{1}$$

where $\vec{x}_w(t) \in \Re^{6x1}$ is a vector of the vehicle position and orientation measured with respect to a world-fixed inertial coordinate frame; $\vec{v}(t) \in \Re^{6x1}$ and $\dot{\vec{v}}(t) \in \Re^{6x1}$ are, respectively, vectors of the vehicle velocity and acceleration in vehicle body coordinates; $\vec{\tau}(t) \in \Re^{6x1}$ is a vector of control forces from thrusters and control surfaces in body coordinates; $M(\vec{x}_w(t), \vec{v}(t))$ is a mass matrix representing both rigid-body mass and velocity-dependent "added mass"; $d(\vec{x}_w(t), \vec{v}(t))$ is a vector of vehicle drag forces; and $b(\vec{x}_w(t))$ is a vector of vehicle buoyancy forces. Note that the velocity in inertial (world) coordinates $\vec{v}_w(t)$, is related to the velocity in body coordinates by a linear transformation of the form $\vec{v}_w(t) = T(\vec{x}_w(t))\vec{v}(t)$ [4].

At present, there is no uniform consensus within the research community on the exact analytical form of the terms comprising $M(\vec{x}_w(t), \vec{v}(t))$, $d(\vec{x}_w(t), \vec{v}(t))$, and $b(\vec{x}_w(t))$, nor for the force vector $\tau(t)$. The few studies that have reported specific instances of (1), e.g. [5], have based their component terms on the David Taylor Model Basin (DTMB) standard submarine equations of motion [4, 3]. These equations represent a finite-dimensional approximation of the infinite-dimensional hydrodynamics.

Although not theoretically justified, in this report we adopt the common practice of further approximat-

0-933957-31-9

Figure 1: Jason 2 is a 3400 kg 6500 meter ROV for oceanographic research, shown on sea-trials in July 2002 aboard the *R.V. Atlantis* on the Juan de Fuca Ridge. Jason 2 was developed and is operated with NSF support for use by the U.S. Oceanographic Community by the National Deep Submergence Facility (NDSF) of the Woods Hole Oceanographic Institution (WHOI).

ing the 6-DOF equations by neglecting off-diagonal entries and coupling terms, tether dynamics, as well as assuming a constant added mass [8, 2]. These simplifications are empirically justified under the operating conditions characterized by slow velocities and modest attitude changes typical of this class of underwater vehicles. The resulting decoupled single DOF dynamical equations take the form

$$\begin{aligned}\tau_i(t) &= m_i\dot{v}_i(t) + d_{Q_i}v_i(t)|v_i(t)| + d_{L_i}v_i(t) + b_i,\\ &\quad m_i > 0;\ d_{L_i}, d_{Q_i} > 0,\end{aligned} \tag{2}$$

or, rewritten,

$$\begin{aligned}\dot{v}_i(t) &= m_i^{-1}\tau_i(t) - m_i^{-1}d_{Q_i}v_i(t)|v_i(t)| - \\ &\quad m_i^{-1}d_{L_i}v_i(t) - m_i^{-1}b_i,\end{aligned} \tag{3}$$

where, for each DOF i, $\tau_i(t)$ is the net control force, m_i is the effective mass, $d_{Q_i}v_i(t)|v_i(t)|$ and $d_{L_i}v_i(t)$ represent the quadratic and linear hydrodynamic drag, respectively, and b_i is the buoyancy. The reader is referred to [10] for a complete derivation of (2).

Using lumped parameters (3) can be written as:

$$\dot{v}_i(t) = \alpha_i\tau_i + \beta_i v_i(t)|v_i(t)| + \mu_i v_i(t) + \nu_i, \tag{4}$$

or written in vector form as

$$\dot{V}(t)_i = \Phi_i^T F(t)_i, \tag{5}$$

where $\Phi_i = [\alpha_i, \beta_i, \mu_i, \nu_i]^T$ is the vector of lumped plant parameters and $F(t)_i = [\tau(t)_i, v_i|v_i|, v_i, 1]^T$ is a

Degree-of-Freedom	Force Moment	Linear Velocity Angular Velocity	Linear Position Angular Position
1: X Translation (Surge)	$\tau_1(t)$	$v_1(t)$	$x_1(t)$
2: Y Translation (Sway)	$\tau_2(t)$	$v_2(t)$	$x_2(t)$
3: Z Translation (Heave)	$\tau_3(t)$	$v_3(t)$	$x_3(t)$
4: Rotation About Z(Yaw/HDG)	$\tau_4(t)$	$v_4(t)$	$x_4(t)$
5: Rotation About Y(Pitch)	$\tau_5(t)$	$v_5(t)$	$x_5(t)$
6: Rotation About X(Roll)	$\tau_6(t)$	$v_6(t)$	$x_6(t)$

Table 1: Nomenclature

non-linear vector of state and the control input $\tau(t)_i$. The lumped parameters are defined in Table 2.

Lumped Parameters	Physical Definition
α_i	m_i^{-1}
β_i	$-m_i^{-1}d_{Q_i}$
μ_i	$-m_i^{-1}d_{L_i}$
ν_i	$-m_i^{-1}b_i$

Table 2: Lumped Parameters

2.2 Least-Squares Parameter Identification

Parameters for the plant (5) enter linearly, and thus can be identified experimentally using standard least-squares techniques. These methods requires values for $v(t)_i$, $\dot{v}(t)_i$, and $\tau(t)_i$ for each DOF i.

Defining $\dot{\bar{V}}_i = [\dot{v}(t_1)_i ... \dot{v}(t_n)_i]_{1\times n}$ and $\bar{F}_i = [F(t_1)_i, \cdots, F(t_n)_i]_{4\times n}$, where $t_1, t_2, \cdots, t_n$ represent the sample times, then from (5) we have

$$\dot{\bar{V}}_i = \Phi_i^T \bar{F}_i. \tag{6}$$

Thus if $\vec{F}$ has rank = 4, then the least-squares solution for the unknown parameter vector Φ_i is given by the standard Moore-Penrose pseudo-inverse

$$\Phi_i = (\dot{\bar{V}}_i \bar{F}_i^T (\bar{F}_i \bar{F}_i^T)^{-1})^T. \tag{7}$$

3 Experimental Setup

These experiments were conducted with the Jason 2 ROV during its first sea-trial deployment from the *R.V. Atlantis* on the Juan de Fuca Ridge in July 2002. This experimental data was collected during vehicle descent and ascent operations, and during vehicle near-bottom bottom operations at a depth of 1650 meters. The vehicle navigation sensors used in these experiments are listed in Table 3. Vehicle x_3 position was measured using a Paroscientific model 8CB7000-I depth sensor. A 1200 kHz RDI Doppler Velocity Log (DVL). Note that the velocities reported by the DVL are the velocities of the DVL instrument itself; they are not the velocities of the origin of the coordinate frame of the ROV. The DVL instrument data, vehicle attitude data from the vehicle's gyro, and measured sensor position and orientation offsets are used by the DVLNAV navigation program to compute the displacement of the vehicle frame of reference in six degrees of freedom [7]. Heading, pitch, and roll angular positions were obtained from an IXSEA Octans 3-axis fiber optic gyro. Vehicle velocity was obtained via direct numerical differentiation of the position signals. During post-experiment processing of the data, a 1/8th Hz 2nd order acausal zero-phase low-pass filter was used to smooth the differentiated signal.

Multiple trials in each DOF were conducted with open-loop thrust profiles or closed-loop reference trajectories comprised of the sum of (a) a sinusoidal reference signal with selected magnitude and frequency and (b) the manual input of the pilot's joystick. Each trial was conducted in a single DOF at a time. Table 4 list the specific trials for the results reported in this paper.

The vehicle's six thrusters each are comprised of a pressure-tolerant Kollmorgen 3-Phase brushless DC motors directly coupled to an Innerspace ducted thruster, with MTS back-EMF based commutating amplifiers providing precise real-time velocity control of the thrusters. The Jason 2 thrusters are normally operated at up to 1650 RPM with a maximum power consumption of about 4.7KW per thruster. A static quadratic thrust model was used in this experimental analysis to estimate the thrust produced by each thruster. Figure 2 shows data from experiments confirming that bollard-pull thrust produced is proportional to the square of the propeller angular velocity. The thruster coefficients were determined to be 0.0402 $Newton/(radian \cdot second)^2$ for forward thrust and 0.0328 $Newton/(radian \cdot second)^2$ for reverse thrust. The authors are aware of more advanced dynamic thruster models, e.g. [6, 1], however these dynamic models require a dynamical thruster characterization not available at the time of these experiments.

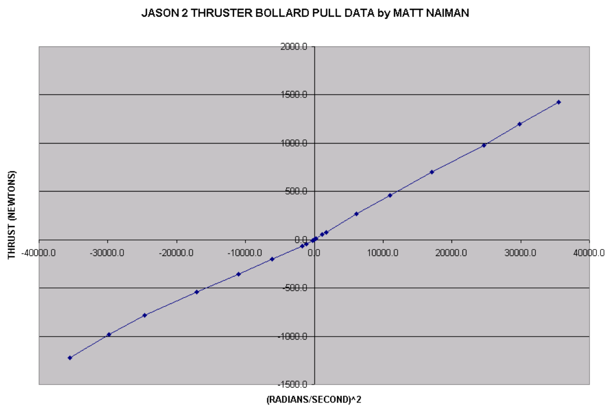

Figure 2: Jason 2 Thruster Data: Bollard pull thrust in $Newtons$ as a function of the square of the propeller angular velocity in $(radians/second)^2$. This experimental data was obtained by WHOI Engineer Matthew Naiman on December 4, 2001.

4 Experimental Results

This section reports the plant model parameters identified from free-motion experimental data using conventional least-squares parameter identification and the identified estimates for the coefficient of quadratic drag, D_q, for the x_3 DOF. We report the following steps: First we state the procedure followed to execute the identification technique. Second, we report the resulting identified plant parameters. Third, we evaluate the quality of the identified plant parameter values by quantitatively comparing experimentally observed plant dynamical performance to that predicted by the identified plant model.

4.1 Decoupled Single Degree-of-Freedom Dynamical Plant Model Identification from Unsteady Dynamical Data

We employed the conventional least-square parameter identification outlined in Section 2.2, to experimentally determine plant parameter values for the Jason 2 ROV. First, dynamic experiments were conducted in the x_1, x_2, x_3, and x_4 DOF. Table 4 reports the experimental trials corresponding to the results reported here. For each experiment, estimates for the plant parameters were determined using the least-squares method. Next numerical simulations of the identified plant model were executed. These simulations employed the actual thruster force/moment logged from the experiments. The simulated model velocity, v_{model_i}, was compared to the actual logged experimental plant velocity, v_{p_i}. The error, for each DOF i, was calculated as $e_i = mean(|v_{model_i} - v_{p_i}|)$. Plots of v_{model_i}, v_{p_i}, and $v_{model_i} - v_{p_i}$ are shown in Figures 3, 4, 5, and 6. The identified parameters that resulted in a stable plant model are listed in Table 5.

4.2 Estimation of Quadratic Drag Coefficient in x_3 Degree of Freedom from Steady-State Experimental Data

As is well known, e.g. [2], it is possible to identify some plant parameters with steady-state (constant velocity) experimental trials. Normal deep-sea ROV deployment includes an extended period of steady-state vertical ascent and descent, thus offering another opportunity for identification the quadratic drag term for the x_3 degree-of-freedom.

This section reports the experiments identification of quadratic drag for the the x_3 degree-of-freedom from steady-state ascent and descent data. As in Section 4.1, a conventional least-square parameter identification method is employed. These experiments consisted of commanding the x_3 DOF thrusters on Jason 2 to hold constant some percentage of their maximum thrust for a predetermined period of time. During this time the ROV reaches a steady state velocity. Given that $\dot{v}_i(t) = 0$, assuming the effect of b_i to be negligible compared to $\tau_i(t)$, and only considering the effects of quadratic drag, (2) yields

$$\tau_i(t) \quad = \quad d_{Q_i} v_i(t)|v_i(t)|, \; d_{Q_i} > 0. \qquad (8)$$

At steady-state, the force exerted by the thrusters is equal to the quadratic drag. For each experiment, estimates of D_q were determined using the least-squares method. Next numerical simulations of the vehicle plant model were executed using the identified parameters. The simulations employed the actual logged force profile from the experiment. The output of the simulation was a velocity, v_{model_3}, which was compared to the actual logged experimental plant velocity, v_{p_3}. The error was calculated as $e_3 = mean(|v_{model_3} - v_{p_3}|)$. The identified parameters that resulted in a stable plant model are listed in Table 6. The mean of the values listed in Table 6 is 5660.6 $N/(m/s)^2$.

4.3 Discussion of Results

Do the identified plant parameters seem reasonable? This section addresses this question.

4.3.1 Mass Parameters

The experimentally identified inertia parameters given in Table 5 represent the the vehicle total mass — the sum of the vehicle dry mass and the vehicle's hydrodynamic added mass. The Jason 2 ROV, Figure 1, has a total dry mass of about 3400 kg. Hydrodynamic added mass is a lumped parameter approximation for the mass of water that is accelerated by the vehicle as the vehicle accelerates through the water column. The added mass parameters seem reasonable for two reasons: First, the experimentally identified inertia parameters indicate that the identified added mass is always positive — in agreement with our analytical expectations. Second, the data indicate that added mass is smallest in the x_1 DOF and largest in the x_3 DOF. This is consistent with the fact that the vehicle's cross-section area is and smallest in the x_1 DOF and largest in the x_3 DOF.

4.3.2 Drag Parameters

The experimentally identified quadratic drag parameters indicate that drag is largest in the x_3 DOF and smallest in the x_1 DOF. The quadratic drag parameters seem reasonable for two reasons: First, the experimentally drag terms are all positive — thus yielding a *stable* plant model in agreement with our analytical expectations. Second, the data indicate that quadratic drag is smallest in the x_1 DOF and largest in the x_3 DOF. This is consistent with the conventional engineering approximation in which quadratic drag is proportional to cross-section area, and the fact that the vehicle's cross-section area is and smallest in the x_1 DOF and largest in the x_3 DOF.

The quadratic drag value obtained for the x_3 DOF with the unsteady dynamic trial data differ significantly from those obtained in the steady-state trials. The subsequent simulations indicate that vehicle models employing quadratic drag parameters obtained from the steady-state experiments more closely agree with the vehicle's actual experimental data. Thus the steady state trials appear to yield superior parameter values for quadratic drag. We surmise that this is a consequence of three effects: First, the steady-state experiments achieved significantly higher peak velocities than the unsteady experiments, thus providing a significantly larger quadratic drag force. Second, the least-square parameter identification of the unsteady data relies on (comparatively noisy) acceleration data in addition to velocity and thrust data. In contrast, the steady-state analysis only requires thrust and velocity data. Thus the analysis of the unsteady data may be degraded by noise in the acceleration data. Third, this preliminary unsteady parameter identification employed a standard unweighted least-square technique. Judicious use of weighted least square methods might yield improved parameter values.

The addition of a linear drag term (i.e. skin friction) did not, in general, result in improved model performance.

4.3.3 Buoyancy Parameters

The buoyancy term is significant principally in the x_3 DOF. This is consistent with the fact that the vehicle was ballasted for positive buoyant in these trials. For other degrees of freedom, the buoyancy term acts as a general error term. In all degrees of freedom, models identified with a buoyancy term outperformed models identified with no buoyancy term.

4.3.4 Comparison of Identified Model Dynamics Response and Experimentally Observed Vehicle Response

With the above identified model parameters, we implemented numerical simulations of the model response to the actual thruster force/moment logged from the experiments.

A comparison of model and experimental response for the unsteady trials is given in Table 5 and Figures 3, 4, 5, and 6. The data indicate good correspondence between model and experiment for the x_2, x_3, and x_4 DOF, and poor agreement for the x_1 DOF. We hope to repeat these experiments in the future both to corroborate the results and to further investigate the discrepancy between model and experiment for the x_1 DOF.

A comparison of model and experimental response for x_3 quadratic drag in the steady-state trials is given in Table 6. The data indicates very good correspondence between model and experimental data — the model velocities generally agree with and experimental vehicle velocities to within 1 $cm/second$.

5 Conclusion

This paper has reported the experimental identification of a decoupled non-linear dynamical plant model for the Jason 2 ROV. The identified model is shown to be generally in agreement with the observed dynamical behavior of the Jason 2 ROV, and will serve as the basis for future work implementing model-based control algorithms aboard the Jason 2 ROV.

6 Acknowledgments

We gratefully acknowledge the collaboration of the Faculty and Staff of the National Deep Submergence Facility and the Deep Submergence Laboratory of the Woods Hole Oceanographic Institution. We are grateful to Mr. Matthew Naiman, Engineer II, of the WHOI Deep Submergence Laboratory, for the thrusters identification data employed in the execution of the Jason 2 control system and the analysis of these experiments. We gratefully acknowledge the support of our research by the National Science Foundation. The Jason 2 vehicle development was supported by the National Science Foundation and the Keck Foundation.

References

[1] R. Bachmayer, L. L. Whitcomb, and M. Grosenbaugh. An accurate four-quadrant nonlinear dynamical model for marine thrusters: Theory and experimental validation. *IEEE Journal of Oceanic Engineering*, 25(1):146–159, January 2000.

[2] M. Caccia, G. Indiveri, and G. Veruggio. Modeling and identification of open-frame variable configuration underwater vehicles. *IEEE Journal of Oceanic Engineering*, 25(2):227–240, April 2000.

[3] J. P. Feldman. DTNSRDC revised standard submarine equations of motion. Technical report, David Taylor Naval Ship Research and Development Center, June 1979. Defense Technical Information Center document #A071804.

[4] M. Gertler and G. Hagen. Standard equations of motion for submarine simulation. Technical report, David Taylor Naval Ship Research and Development Center, June 1967. Defense Technical Information Center document #653861.

[5] A. J. Healey and D. Lienard. Multivariable sliding mode control for autonomous diving and steering of unmanned underwater vehicles. *IEEE Journal of Oceanic Engineering*, 18(3):327–339, July 1993.

[6] A. J. Healey, S. M. Rock, S. Cody, D. Miles, and J. P. Brown. Toward an improved understanding of thruster dyamics for underwater vehicles. *IEEE Journal of Oceanic Engineering*, 20(4):354–61, October 1995.

[7] J. C. Kinsey and L. L. Whitcomb. Preliminary field experience with the DVLNAV integrated navigation system for manned and unmanned submersibles. In *Proceedings of the 1st IFAC Workshop on Guidance and Control of Underwater Vehicles: GCUV 2003*, 2003. Accepted, to appear.

[8] A. T. Morrison III and D. R. Yoerger. Determination of the hydrodynamic parameters of an underwater vehicle during small scale, nonuniform, 1-dimensional translation. In *Proceedings of IEEE/MTS OCEANS'93*, pages 277–282, October 1993.

[9] D. Smallwood, R. Bachmayer, and L. Whitcomb. A new remotely operated underwater vehicle for dynamics and control research. In *Proceedings of the 11th International Symposium on Unmanned Untethered Submersible Technology*, pages 370–377, Durham, NH, USA, 1999.

[10] D. A. Smallwood. *Advances In Dynamical Modeling and Control of Underwater Robotic Vehicles.* PhD thesis, The Johns Hopkins University, Baltimore, MD, USA, 2003.

[11] D. A. Smallwood and L. L. Whitcomb. Preliminary experiments in the adaptive identification of dynamically positioned underwater robotic vehicles. In *Proceedings of the 2001 IEEE/RSJ International Conference on Intelligent Robots and Systems*, pages 1803–1810, Maui, HI, USA, 2001.

[12] D. A. Smallwood and L. L. Whitcomb. Toward model based dynamic positioning of underwater robotic vehicles. In *Proceedings of IEEE OCEANS' 2001*, pages 1106–1114, Honolulu, HI, USA, 2001.

Variable	Sensor	Precision	Update Rate
XYZ Velocity	1200 kHz RDI DVL	0.3 mm/s	10 Hz
Depth	Paroscientific	7 cm	0.6 Hz
Heading	IXSEA Octans	0.1 deg.	10 Hz
Roll and Pitch	IXSEA Octans	0.1 deg.	10 Hz

Table 3: Instrumentation

DOF	Trajectory Type	Peak Magnitude	Frequency
1 (x_1)	Open Loop Thrust	1800 N	0.785 rad/s (1/8 Hz)
2 (x_2)	Open Loop Thrust	1500 N	0.3925 rad/s (1/16 Hz)
3 (x_3)	Closed Loop Position and Velocity	0.5 m	0.3925 rad/s (1/16 Hz)
4 (x_4)	Open Loop Thrust	2000 N-m	1.0472 rad/s (1/6 Hz)

Table 4: Jason 2 Dynamics Trials - July 2002

Degree of Freedom	α_i	β_i	μ_i	ν_i	Error e_i
1 (x_1)	7.71e-5	-1.72e-1	0	1.97e-2	0.116 m/s
2 (x_2)	5.29e-5	-4.86e-1	0	-4.06e-3	0.0401 m/s
3 (x_3)	4.93e-5	-8.07e-1	0	-4.58e-4	0.0387 m/s
4 (x_4)	9.05e-5	-1.48	0	-1.06e-2	0.0325 rad/s 1.86 deg/s
Degree of Freedom	Inertia	D_Q	D_L	Buoyancy	
1 (x_1)	12970.2 [kg]	2230.9 $[N/(m/s)^2]$	0	-255.5 [N]	
2 (x_2)	18903.6 [kg]	9187.1 $[N/(m/s)^2]$	0	76.7 [N]	
3 (x_3)	20283.9 [kg]	16369.2 $[N/(m/s)^2]$	0	9.29 [N]	
4 (x_4)	11049.7 [kg m^2]	16353.6 $[N-m/(rad/s)^2]$	0	117.1 [N-m]	

Table 5: Jason 2 SDOF Decoupled Dynamical Plant Lumped Parameter Values from Unsteady Dynamic Trials.

Thrust Level	Direction of Travel	D_{Q_3} $[N/(m/s)^2]$	Error e_3
30%	Down	6682.0	0.0101 m/s
60%	Down	5276.4	0.0103 m/s
80%	Down	6879.1	0.00491 m/s
100%	Down	6502.1	0.00844 m/s
30%	Up	3276.8	0.003804 m/s
60%	Up	6025.6	0.00390 m/s
100%	Up	4981.9	0.00373 m/s

Table 6: Jason 2 x_3 DOF Quadratic Drag Coefficient Estimates from Steady-State Ascent/Descent Trials.

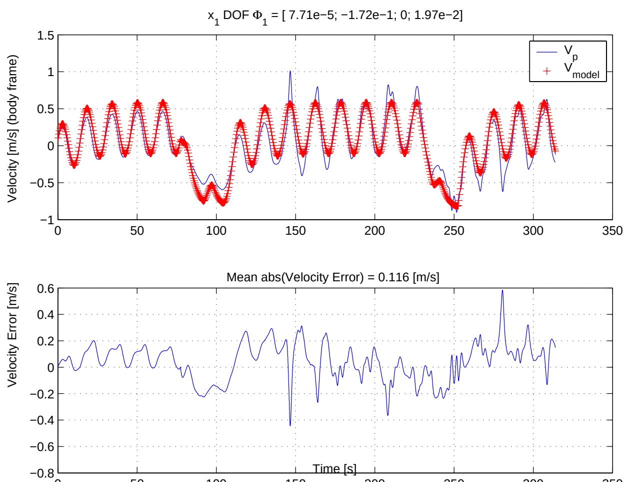

Figure 3: x_1 DOF: Comparison of the performance of the least-squares identified plant model, (5), and actual experimental data. The plots show model-simulated and actual velocity versus time (top graph); and the velocity error between simulated and experimentally observed velocities (bottom graph).

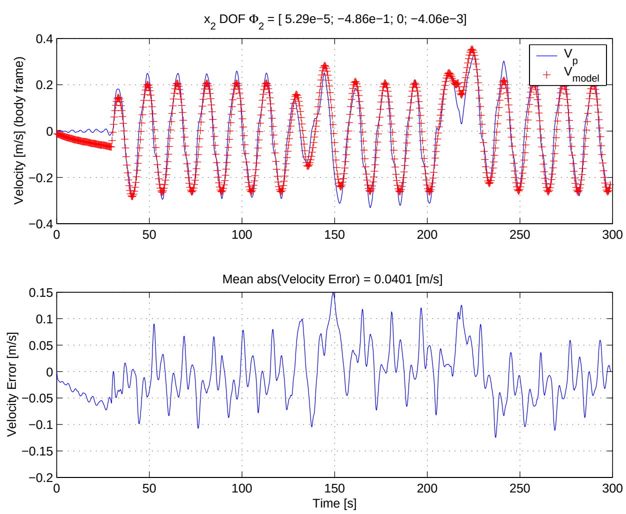

Figure 4: x_2 DOF: Comparison of the performance of the least-squares identified plant model, (5), and actual experimental data. The plots show model-simulated and actual velocity versus time (top graph); and the velocity error between simulated and experimentally observed velocities (bottom graph).

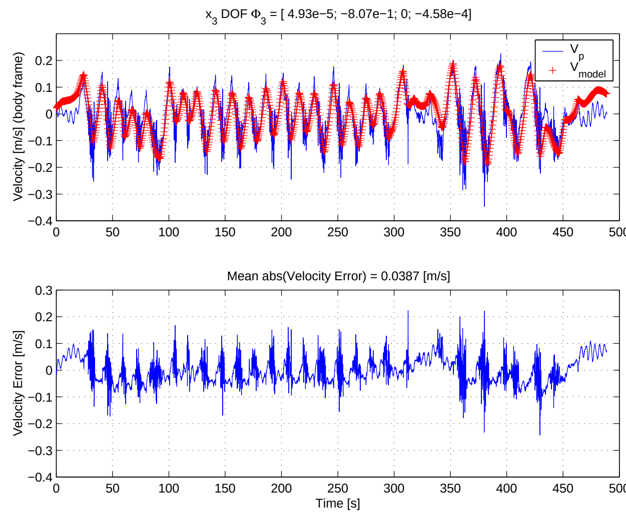

Figure 5: x_3 DOF: Comparison of the performance of the least-squares identified plant model, (5), and actual experimental data. The plots show model-simulated and actual velocity versus time (top graph); and the velocity error between simulated and experimentally observed velocities (bottom graph).

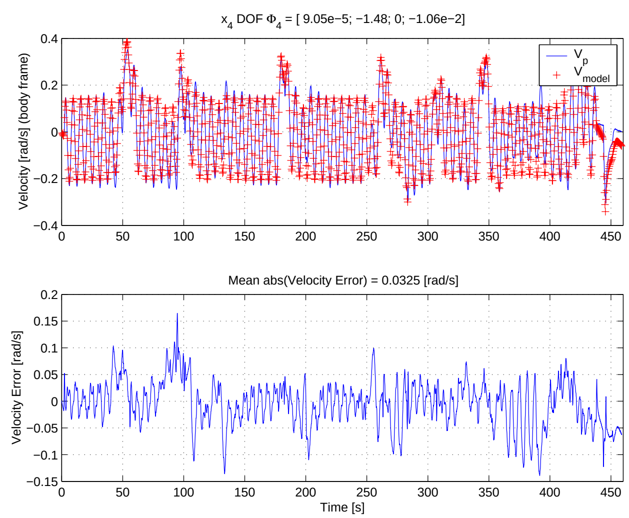

Figure 6: x_4 DOF: Comparison of the performance of the least-squares identified plant model, (5), and actual experimental data. The plots show model-simulated and actual velocity versus time (top graph); and the velocity error between simulated and experimentally observed velocities (bottom graph).